analytical chemistry

pubs.acs.org/ac Article

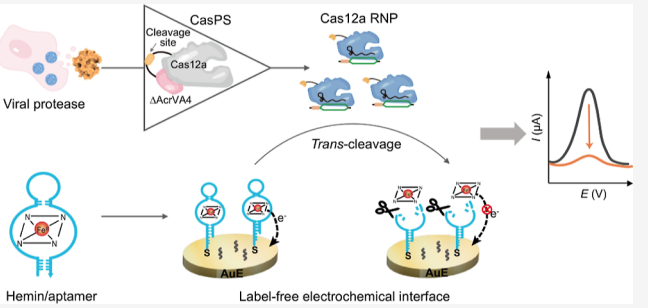
CRISPR/Cas12a Protein Switch Powered Label-Free Electrochemical Biosensor for Sensitive Viral Protease Detection

Tianyi Zhang,‖ Yingying Zhao,‖ Cong Zhu, Xi Zhu, Xiaohua Zhu,* Ye Qiu, Zhou Nie, and Chunyang Lei*

Cite This: https://doi.org/10.1021/acs.analchem.5c00547 Read Online

ACCESS | Metrics & More | Article Recommendations | Supporting Information

ABSTRACT: Viral proteases are critical molecular targets in viral pathogenesis, representing pivotal biomarkers for understanding viral infection mechanisms and developing antiviral therapeutics. This study introduces a label-free electrochemical biosensor that enables sensitive viral protease detection by integrating protease-responsive CRISPR/Cas protein switches (CasPSs) with a hemin aptamer-functionalized electrochemical interface. The biosensor's mechanism relies on viral protease-mediated proteolysis, which leads to the release of active Cas12a proteins from CasPSs and generates amplified electrochemical responses through continuous cleavage of immobilized redox-active hemin/aptamer complexes. This biosensor achieved specific hepatitis C virus NS3/4A protease sensing with femtomolar sensitivity and could be readily expanded to other viral proteases by replacing the CasPS module. The feasibility of this biosensor was demonstrated by monitoring enterovirus 71 3C protease activities in virus-infected cell samples with different viral loads and postinfection times. This study provides a promising strategy for integrating CRISPR biosensing with electrochemical platforms, offering a helpful analytical tool for viral infection monitoring and antiviral drug screening.



Downloaded via SHANGHAI NORMAL UNIV on April 2, 2025 at 04:03:00 (UTC).
See https://pubs.acs.org/sharingguidelines for options on how to legitimately share published articles.

INTRODUCTION

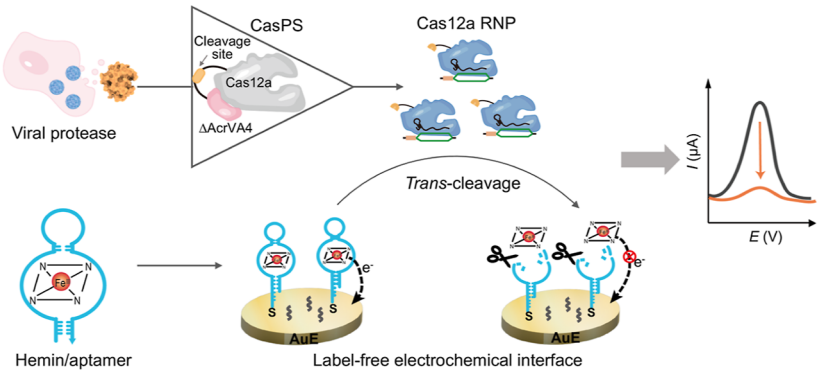
The development of robust methodologies for detecting viral infections and screening antiviral drugs is crucial for addressing contemporary and emerging infectious disease challenges.[1−3] Viral proteases, which catalyze polyprotein peptide chain hydrolysis, play pivotal roles during viral pathogenesis.[4] These enzymes facilitate critical processes such as viral protein cleavage, viral particle release, modification of cell surface receptors, and modulation of immune responses.[5−7] For instance, 3C and 3C-like (3CL) cysteine proteases, principal proteolytic enzymes found in coronaviruses, picornaviruses, and enteroviruses, are involved in the proteolytic processing of polyproteins and interference with the cellular processes of host cells.[8] Due to their specificity and critical role in viral infection, proteases represent compelling targets for antiviral drug development.[9−12] The 3C and 3CL proteases are particularly important drug targets in the development of antiviral therapies. Several drugs targeting the 3C or 3CL proteases have been developed and tested in clinical trials. Examples include rupintrivir for human rhinovirus (HRV) and nirmatrelvir and ensitrelvir for severe acute respiratory syndrome coronavirus 2 (SARS-CoV-2).[9,12] Furthermore, viral protease activity serves as a reliable indicator of the viral infection process, and studies have used viral proteases as markers to monitor viral infection.[13,14] Therefore, developing highly sensitive viral protease assays is crucial for elucidating the mechanism of viral infection and facilitating the development of antiviral drugs.

To monitor the active biological state of viral proteases, researchers typically employ chemically modified substrate peptide probes to profile their proteolytic activity.[15] These peptides, functionalized with organic dyes or nanomaterials, generate measurable fluorescent or colorimetric signals in response to protease activity.[16−18] However, these methods are constrained by limited sensitivity due to the absence of signal amplification mechanisms.[19] Recently, RNA-guided CRISPR/Cas systems have been repurposed as versatile biosensing tools due to their inherent nuclease activity-derived signal amplification capacity.[20−22] Particularly, the Class 2 Type VI Cas12a enzyme exhibits high collateral cleavage (trans-cleavage) activity, capable of digesting nearby random single-stranded DNA (ssDNA) sequences with high turnovers.[23] This target-activated trans-cleavage activity endows Cas12a with integrated functionalities, from molecular recognition to signal conversion and amplification. By using chemically modified

Received: January 23, 2025
Revised: March 27, 2025
Accepted: March 28, 2025

ACS Publications © XXXX American Chemical Society

Scheme 1. Schematic Illustrations of the CasPS-Powered Label-Free Electrochemical Biosensor for Viral Protease Detection



ssDNA for signal reporting, the CRISPR-Cas12a system has emerged as a powerful biosensing platform for advanced nucleic acid diagnostics.[24,25] Moreover, CRISPR-Cas12a-mediated signal reporting systems have been exploited as a versatile and efficient signal amplification platform for diverse non-nucleic acid analytes by combining with other biorecognition modules.[26−29] Recently, our group expanded Cas12a's biosensing capabilities by engineering its responsiveness toward specific viral proteases.[30] These protease-responsive Cas12a enzyme switches offer an attractive tool for sensitive protease activity assays, while their integration with advanced measurement techniques remains to be fully explored.

Electrochemical techniques offer distinct advantages, including high sensitivity, rapid response, operational simplicity, and cost-effectiveness.[31] Their integration with CRISPR/Cas systems has established new paradigms in biosensing.[32,33] Particularly, label-free electrochemical CRISPR biosensors have garnered increasing attention due to their simplified signal generation mechanisms.[34] Here, we present a label-free electrochemical biosensor that combines an electrochemical interface with protease-responsive Cas12a protein switches (CasPSs) for amplified viral protease detection. We first demonstrate that the complexes formed by hemin and a recently selected hemin aptamer can effectively report Cas12a trans-cleavage activity through colorimetric and electrochemical signaling, exhibiting significantly improved performance compared to conventional hemin/G4 complexes. As illustrated in Scheme 1, the CasPS module is engineered through fusion of Cas12a to its truncated anti-CRISPR counterpart (ΔAcrVA4) via a peptide linker incorporating the substrate sequence of the target viral protease. Each proteolytic event of the CasPS by the target viral protease generates an active Cas12a, which continuously cleaves the hemin/aptamer complexes immobilized on the electrode to produce amplified electrochemical responses. Employing HCV NS3/4A protease as a model, this label-free electrochemical sensor achieves specific protease detection with femtomolar sensitivity. By fine-tuning the CasPS module, the target scope of this electrochemical biosensor could successfully expand to different viral proteases. Moreover, the sensor demonstrates remarkable capability in detecting viral 3C protease activity within the lysates from cells infected with enterovirus 71 (EV71). Furthermore, we assess the sensor's feasibility in monitoring 3C protease activities during the infection process of EV71 infection at varying viral loads and postinfection times. Therefore, this study establishes a new electrochemical biosensor for sensitive viral protease analysis, highlighting its potential applications in viral disease diagnostics and antiviral drug development.

EXPERIMENTAL SECTION

Chemicals. Proteases, including HRV type 14 3C protease, tobacco etch virus (TEV) protease, and 3C cysteine proteinase, were obtained from Beyotime Biotechnology (Shanghai, China). Thrombin (Thr) and matrix metalloproteinase-2 (MMP2) were purchased from Sigma-Aldrich (Saint Louis, MO, USA). TMB One Solution (HRP-based ELISA) was acquired from Yisheng Bio (Shanghai, China). Additional reagents were sourced from various manufacturers: isopropyl β-D-thiogalactoside (IPTG), imidazole, kanamycin, dithiothreitol (DTT), and glycerol from Aladdin Biochemical Technology Co., Ltd. (Shanghai, China); heparin sodium and tris hydrochloride from Sangon Biotech Co., Ltd. (Shanghai, China); hemin and SYBR Green II from Thermo Scientific (Waltham, MA, USA). Cell culture materials, including Dulbecco's modified Eagle's medium (DMEM) and Roswell Park Memorial Institute (RPMI)-1640 media, trypsin, and fetal bovine serum (FBS), were obtained from Invitrogen (Gibco, USA). HPLC-purified RNA and DNA oligonucleotide sequences (detailed in Table S1) were synthesized and purified by General Biology Co., Ltd. (Anhui, China) and Sangon Biotech Co., Ltd. (Shanghai, China), respectively. Stock solutions (100 μM) of oligonucleotides were prepared using DEPC-treated water and stored at −20 °C until use. All chemicals were of analytical grade, and solutions were prepared using ultrapure water (18.2 MΩ·cm).

Protein Expression and Purification. Protein expression and purification procedures for LbCas12a, CasPSs, and HCV NS3/4A protease followed previously established protocols.[35] The expression vectors pET28a(+)-lbCas12a, pET28a(+)-$CasPS_{NS3/4A}$, pET28a(+)-$CasPS_{3C}$, and pET28a(+)-$CasPS_{TEV}$ were obtained from GenScript Biotech Corporation (Nanjing, China). For LbCas12a production, *Escherichia coli* (*E. coli*) Rosetta (DE3) cells were induced with 0.2 mM IPTG and cultured at 16 °C for 16 h. His-tagged LbCas12a was isolated using nickel affinity chromatography, with sequential application of wash buffer (50 mM Tris−HCl, 1.5 M NaCl, 30 mM imidazole, pH 8.0) and elution buffer (50 mM Tris−HCl, 1.5 M NaCl, 600 mM imidazole, pH 8.0). Final purification involved buffer exchange using demineralization buffer (50 mM Tris−HCl, 150 mM NaCl, 2 mM DTT, 10% glycerol, pH 8.0). The expression of CasPSs adopted the same procedure.

HCV genotype 1a NS3/4A protease was expressed in *E. coli* cells induced with 0.5 mM IPTG at 25 °C for 16 h. Cell lysates

https://doi.org/10.1021/acs.analchem.5c00547
Anal. Chem. XXXX, XXX, XXX−XXX

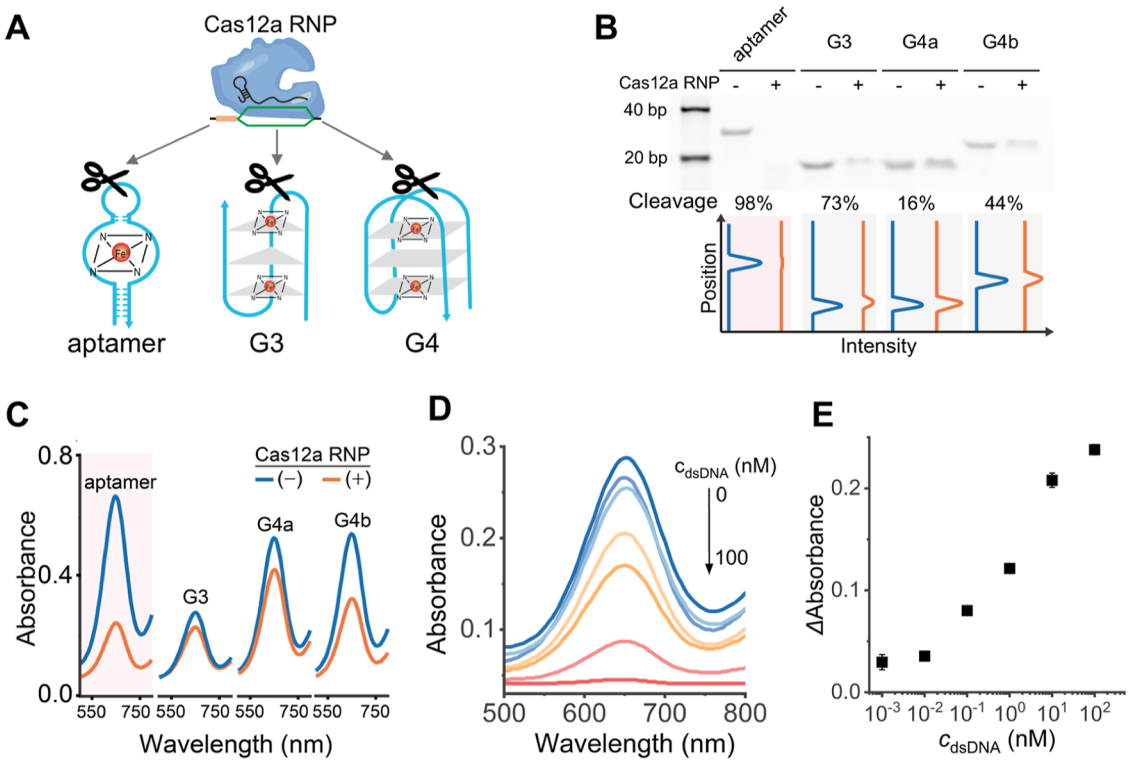


Figure 1. Reporting of Cas12a's trans-cleavage activity based on hemin aptamer. (A) Assessment of the trans-cleavage of various hemin-binding DNA scaffolds by Cas12a RNPs. (B) Gel electrophoresis analysis of the cleavage of the aptamer, G3, G4a, and G4b by the activated Cas12a RNPs. (C) Colorimetric signals resulting from the oxidation of TMB catalyzed by the hemin/DNA complexes, with and without prior treatment with activated Cas12a RNPs. (D) Colorimetric signals produced by the hemin/aptamer-based CRISPR/Cas12a biosensing system in response to varying DNA target concentrations. The DNA concentrations were 0, 0.001, 0.01, 0.1, 1, 10, and 100 nM; aptamer, 1 μM; hemin, 1.2 μM; and Cas12a/crRNA, 100 nM. (E) Changes in absorbance at 652 nm (ΔAbs) corresponding to different DNA concentrations. Data points are expressed as mean ± standard deviation (SD, n = 3).

in resuspension buffer (50 mM HEPES, 500 mM NaCl, 20 mM imidazole, pH 7.6) underwent Ni-NTA agarose chromatography, followed by buffer exchange into desalination buffer (50 mM HEPES, 150 mM NaCl, 1 mM DTT, 10% glycerol, pH 7.6).

For electrophoretic analysis, proteins were diluted to appropriate concentrations (1 μM LbCas12a and CasPS; 5 μM NS3/4A protease) in DEPC water, combined with SDS-PAGE loading buffer, and processed for gel-shift assay. Samples (10 μL) were resolved on 10% denaturing polyacrylamide gels at 110 V for 2 h and visualized using an Azure 300Q imaging system (Azure Biosystems Inc., USA).

Preparation of the Electrochemical Biosensor. The bare gold electrode (AuE) was purified by a piranha solution and polished with 0.05 μm alumina slurry. After cleaning, the electrode underwent cyclic scanning between −0.3 to 1.5 V in 0.5 M H_2SO_4 solution until a stable voltammogram was attained. Afterward, the electrode was immersed into a stabilizing buffer (10 mM HEPES, 0.5 M $NaClO_4$, and 1.0 mM TCEP, pH 7.0) with 2 μM aptamer for 2 h. The AuE was then rinsed with purified water to remove loosely bound probes, followed by overnight immersion in a 2 mM solution of 6-mercaptohexyl alcohol (MCH) to ensure secure attachment to the gold surface, preventing nonspecific adsorption. After washing and drying, 7 μL of a 100 μM hemin solution was incubated in the buffer for 30 min.

Procedure for Electrochemical Analysis. All the electrochemistry experiments were performed in a three-electrode cell using a CHI660A CH electrochemical workstation (Shanghai, China). The AuE was used as the working electrode, and the saturated calomel electrode (SCE) and platinum electrode served as reference electrode and auxiliary electrode, respectively. Electrochemical impedance spectroscopy (EIS) was performed across a frequency range of 0.1 Hz to 100 kHz, with an applied amplitude of 5.0 mV and a potential of 0.22 V referenced against the SCE. The cyclic voltammetry (CV) was carried out in 0.1 M KCl solution containing 5.0 mM $[Fe(CN)_6]^{3-/4-}$ by scanning the potential from −0.2 to 0.6 V under a scan rate of 50 mV·s^{-1}. All electrochemical measurements were carried out at room temperature (25 ± 2 °C).

Preparation of EV71-Infected Cell Lysates. Human embryonic kidney (HEK 293T) cells were cultured in high-glucose (4.5 g/L) DMEM supplemented with 10% FBS, 100 U/mL penicillin, and 100 μg/mL streptomycin. EV71 virus purification was performed following established protocols from previous literature.[36] HEK293T cells were infected with EV71 viruses at varying titers for a specified duration, then washed with phosphate-buffered saline (PBS) and lysed using radioimmunoprecipitation assay (RIPA) buffer composed of 150 mM sodium chloride, 1% Nonidet P-40, 0.5% sodium deoxycholate, 0.1% sodium dodecyl sulfate (SDS), and 50 mM Tris−HCl (pH 8.0). Then, the lysates were supplemented with 2 g/mL aprotinin, 2 g/mL leupeptin, 20 g/mL phenylmethylsulfonyl fluoride, and 2 mM DTT to retain protease activity.

https://doi.org/10.1021/acs.analchem.5c00547
Anal. Chem. XXXX, XXX, XXX−XXX

RESULTS AND DISCUSSION

Reporting of Cas12a's Trans-Cleavage Activity Based on Hemin Aptamer. CRISPR/Cas12a ribonucleoprotein (RNP) retains its active conformation following cis-cleavage of target DNA and exhibits robust trans-cleavage activity toward ssDNA, which has been repurposed as a versatile signal amplification platform in biosensing.[37] By utilizing fluorophore- or redox-modified ssDNA substrates, the presence of target analytes can be converted into amplified fluorometric or electrochemical signal outputs.[38] Although this strategy is effective, the preparation of dual-labeled ssDNA substrates typically requires complex synthesis and purification procedures. To overcome this limitation, we sought to construct DNA substrate probes by leveraging the noncovalent interactions between aptamers and their ligands. In this context, the recently selected hemin aptamer emerges as an ideal candidate,[38] owing to hemin's diverse functionalities, particularly its catalytic and electrochemical activities.

To evaluate the potential of hemin/aptamer complexes as reporters for Cas12a RNP trans-cleavage activity, we investigated the susceptibility of hemin/aptamer complexes to cleavage by activated Cas12a RNPs (Figure 1A). To this end, we selected various hemin-binding DNA scaffolds, including G-triplex (G3), two G-quadruplexes (G4a and G4b), and hemin aptamer for evaluation (Figure S1). Subsequently, using the widely used *Lachnospiraceae* bacterium ND2006 Cas12a as the model (Figure S2), these DNA scaffolds were incubated with activated Cas12a RNPs and analyzed by gel-shift assay. Gel analysis revealed that exposure to activated Cas12a RNPs resulted in complete degradation of the aptamer band, with a cleavage efficiency of 98% (Figure 1B). In comparison, G3, G4a, and G4b structures exhibited lower cleavage efficiencies of 73%, 16%, and 44%, respectively. This marked difference in cleavage efficiency suggests that the stem-loop structured aptamer is more susceptible to Cas12a-mediated degradation compared to conventional heme-binding motifs such as G3 and G4, likely due to Cas12a's preferential recognition of hairpin DNA structures.[39]

Additionally, the hemin/aptamer complexes demonstrate robust peroxidase-like activity, catalyzing the oxidation of 3,3′,5,5′-tetramethylbenzidine (TMB) to its blue-colored oxidized form. This property enables the colorimetric detection of Cas12a's trans-cleavage activity. To evaluate this potential, the formation of hemin/DNA complexes was confirmed by the appearance of red-shifted Soret bands in the absorption spectra (Figure S3). Then, the signal reporting capacities of hemin/aptamer, hemin/G3, and hemin/G4s were assessed based on the absorbance changes of oxidized TMB (oxTMB) at 652 nm. As illustrated in Figure 1C, although all hemin/DNA complexes showed reduced colorimetric signals following treatment with activated Cas12a RNPs, the hemin/aptamer system exhibited the most pronounced decrease in absorbance, from 0.67 to 0.25. These findings indicate that hemin/aptamer complexes are superior reporters of Cas12a RNP's trans-cleavage activity, establishing a novel substrate probe for advanced CRISPR biosensing. Therefore, we developed a colorimetric CRISPR assay using hemin/aptamer complexes as reporting probes. Using a fragment of the *E. coli* M13 bacteriophage gene III as the target sequence, we assessed the response of this colorimetric CRISPR assay across gradient target concentrations. The absorbance decreased proportionally with increasing target concentrations from 0 to 100 nM (Figure 1D). By plotting the absorbance changes at 652 nm (ΔAbs) toward different target concentrations (Figure 1E), we demonstrated that this colorimetric CRISPR bioassay could detect target concentrations as low as 1 pM, which is significantly more sensitive than conventional fluorescent CRISPR assays (30 pM, Figure S4). These findings demonstrate the efficacy of hemin aptamer as a reporter for Cas12a's trans-cleavage activity.

Coupling of CasPS with Hemin Aptamer for Colorimetric Protease Detection. Having demonstrated the efficacy of hemin/aptamer complexes in reporting Cas12a's trans-cleavage activity, we explored their application in developing sensitive viral protease bioassays. Our previous research established several protease-responsive CasPSs through computational chemistry-directed rational protein interface engineering.[30] These CasPSs enable the conversion of each viral protease-mediated proteolysis event into an activated Cas12a RNP, offering a powerful tool for the detection of viral proteases. The amalgamation of CasPSs with hemin/aptamer-based probes could potentially elevate detection sensitivity. To validate this approach, we used the protease of the HCV NS3/4A as a model. We expressed $CasPS_{NS3/4A}$ and confirmed its reactivity to HCV NS3/4A protease via SDS-PAGE analysis. The emergence of a band corresponding to the molecular weight of Cas12a signaled the effective release of Cas12a from $CasPS_{NS3/4A}$ through HCV NS3/4A protease-mediated proteolysis (Figure S5).

Subsequently, the activity of the released Cas12a was reported by the peroxidase-like hemin/aptamer complex. We established a colorimetric assay for HCV NS3/4A protease detection by measuring absorbance changes in the detection system (Figure 2A). As depicted in Figure 2B, the absorbance at 652 nm proportionally decreased as HCV NS3/4A protease concentration increased from 1 pM to 10 nM. The response signal displayed a linear relationship with the logarithm of NS3/4A protease concentration in the range of 50 pM to 10 nM. The limit of detection (LOD) was calculated to be 22.6

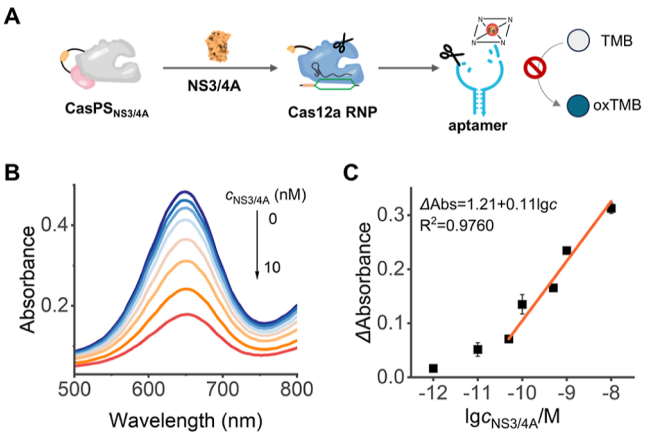


Figure 2. Coupling CasPS with hemin aptamer for colorimetric protease detection. (A) Schematic representation of the colorimetric detection of HCV NS3/4A protease utilizing CasPS and hemin aptamer. (B) Colorimetric signals produced by the CRISPR biosensing system in response to varying concentrations of NS3/4A. NS3/4A concentrations, 0, 0.001, 0.01, 0.05, 0.1, 0.5, 1, and 10 nM; aptamer, 1 μM; hemin, 1.2 μM; $CasPS_{NS3/4A}$, 40 nM; and dsDNA, 50 nM. (C) Changes in absorbance at 652 nm (ΔAbs) corresponding to different NS3/4A concentrations. Data points represent mean ± SD (n = 3).

https://doi.org/10.1021/acs.analchem.5c00547
Anal. Chem. XXXX, XXX, XXX−XXX

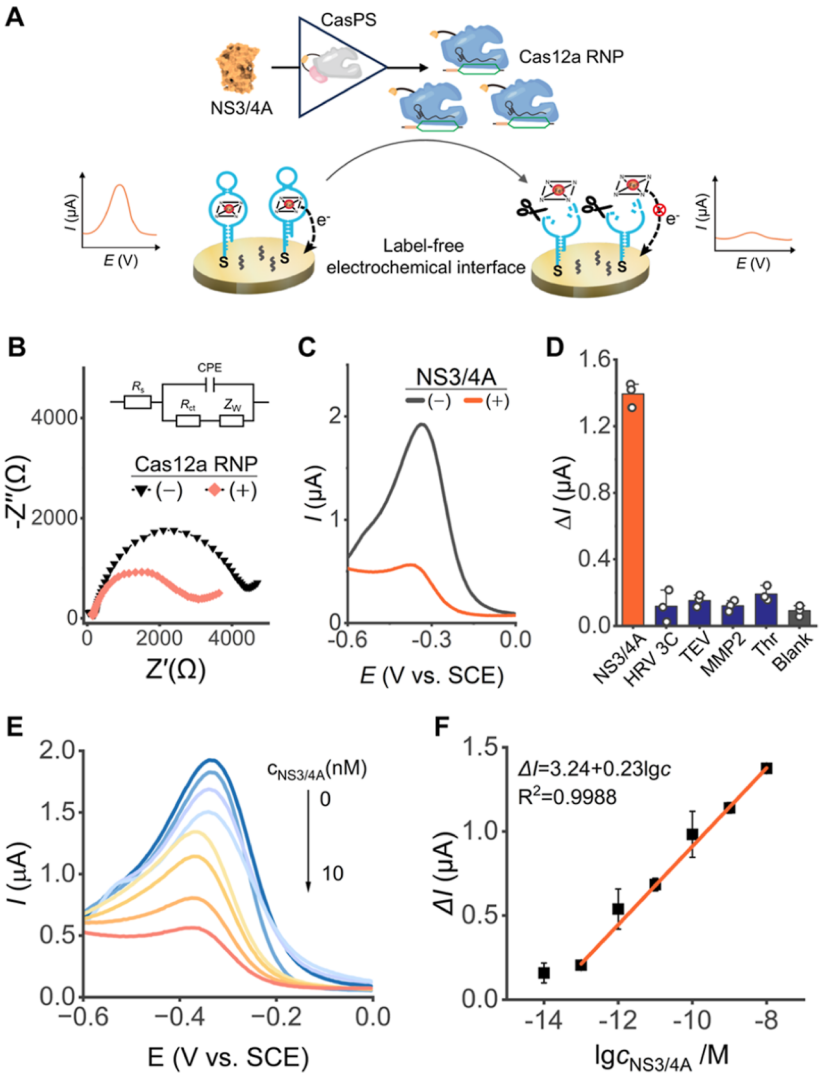


Figure 3. CasPS-powered electrochemical sensors for label-free viral protease detection. (A) Schematic representation of the electrochemical detection of HCV NS3/4A protease based on $CasPS_{NS3/4A}$ activation. (B) EIS of the electrochemical interface with and without the treatment with Cas12a RNPs. The inset illustrates the equivalent circuit used to fit the electrochemical impedance data. R_s and R_{ct} represent the solution resistance and charge transfer resistances, respectively. Z_W denotes the Warburg impedance resulting from the diffusion of ions from the electrolyte bulk to the interface, while CPE indicates the constant phase element of the electrode surface/solution interface. (C) DPV curves of $CasPS_{NS3/4A}$ electrochemical biosensors in the absence (gray) and presence (orange) of HCV NS3/4A proteases. (D) Electrochemical response demonstrating the selectivity of the system toward HCV NS3/4A protease compared to other proteases, including HCV NS3/4A protease (1 nM), HRV 3C protease (100 nM), TEV protease (100 nM), MMP2 (100 nM), and thrombin (Thr, 100 nM). (E) Response of the sensor's DPV signal to varying concentrations of HCV NS3/4A protease. $CasPS_{NS3/4A}$, 40 nM; crRNA, 40 nM; and dsDNA, 10 nM. (F) Linear fitting of the responses of HCV NS3/4A protease to the DPV signal change (ΔI) at different concentrations. ΔI is defined as the blank value minus the value of the blank group. Data points represent mean ± SD (n = 3).

pM according to the 3σ rule,[40] where σ represents the standard deviation of blank samples. These results demonstrate that the coupling of CasPS with the hemin/aptamer complex enables highly sensitive viral protease detection.

CasPS-Powered Electrochemical Sensors for Label-Free Viral Protease Detection. Electrochemical testing techniques present significant advantages, including high sensitivity, rapid response, operational simplicity, and cost-effectiveness.[31] Consequently, exploring the potential of CasPS for developing electrochemical protease sensors is particularly promising. Leveraging hemin's intrinsic redox-active properties, a novel label-free electrochemical interface can be constructed using hemin/aptamer complexes. The viral protease-mediated proteolysis facilitates the release of active Cas12a from CasPS, which induces measurable electrochemical signal alterations through the progressive cleavage of hemin/aptamer complexes (Figure 3A).

Thus, the rational integration of CasPS with a hemin/aptamer-based electrochemical interface offers a robust approach to developing label-free biosensors for viral protease detection. To achieve this, we first constructed a hemin/aptamer-based electrochemical interface. The hemin aptamer, modified with a thiol group at the 5′-terminus, self-assembled on the surface of a AuE through the formation of Au−S bonds, after which the surface was blocked with MCH. The electrochemical interface was then fabricated by hemin binding. Subsequently, we utilized EIS and CV to characterize each step of the electrochemical interface's assembly. The charge transfer resistance (R_{ct}) of the gold electrode progressively increased from 118.8 Ω to 2838 Ω following

https://doi.org/10.1021/acs.analchem.5c00547
Anal. Chem. XXXX, XXX, XXX−XXX

aptamer probe modification (Figure S6A, curves a to b). Subsequent replacement of the nonspecific adsorption probe with MCH further elevated the R_{ct} to 3450 Ω (curve c). Finally, incubation with hemin resulted in a marked interfacial impedance increase, yielding an R_{ct} of 4367 Ω. Similarly, the bare AuE exhibited a pair of well-defined redox peaks (Figure S6B curve a), indicating its inherent electron transfer efficiency. Subsequent stepwise surface modification through aptamer immobilization (curve b), MCH treatment (curve c), and hemin functionalization (curve d) progressively attenuated the CV response signal intensity.

Next, the accessibility of the hemin/aptamer-based electrochemical interface to Cas12a RNPs was subsequently evaluated. The accessibility of the hemin/aptamer-based electrochemical interface to Cas12a RNPs was systematically evaluated. Upon treatment of the electrode with activated Cas12a RNPs, the R_{ct} decreased from 4367 Ω to 2623 Ω (Figure 3B). This observation indicated that Cas12a RNPs could efficiently cleave the immobilized hemin/aptamer complexes, generating distinct electrochemical responses. Subsequently, the electrochemical interface was integrated with $CasPS_{NS3/4A}$ to develop a label-free viral protease biosensor, with the electrochemical response determined by differential pulse voltammetry (DPV). As illustrated in Figure 3C, pretreatment of $CasPS_{NS3/4A}$ with HCV NS3/4A protease resulted in a 74% reduction of the DPV peak current corresponding to the reductive peak of hemin.[41,42] Notably, no significant current variations were observed when $CasPS_{NS3/4A}$ was exposed to other viral proteases, such as HRV 3C protease and TEV protease, as well as physiology/pathology-related proteases, like MMP2 and thrombin (Figure 3D), demonstrating the biosensor's good selectivity.

The surface density of aptamers immobilized at the interface critically determines the capture efficiency of hemin molecules, directly impacting the electrochemical signal generation. Consequently, we systematically optimized the aptamer concentration during electrode immobilization. As illustrated in Figure S7, DPV signals for hemin demonstrated a progressive increase and subsequent stabilization when aptamer concentrations were incrementally varied from 0.1 μM to 2 μM, with a notable plateau observed between 1.5 and 2 μM. Based on these findings, an aptamer concentration of 2 μM was selected as the optimal parameter for subsequent experimental procedures.

Under the optimized condition, the electrochemical responses of HCV NS3/4A protease at varying concentrations were evaluated using the CasPS-powered label-free electrochemical biosensor. As the HCV NS3/4A protease concentration increased from 10 fM to 10 nM, the DPV peak current demonstrated a gradual decline (Figure 3E). A linear relationship was observed between the DPV peak current change (ΔI) and the logarithm of HCV NS3/4A protease concentration, ranging from 100 fM to 10 nM, with the linear regression equation: $\Delta I = 3.24 + 0.23 \lg c$ ($R^2 = 0.9988$). Applying the 3σ rule, the LOD was determined to be 142.0 fM. The intra-assay relative standard deviation (RSD) was 2.2% across six biosensors within the same batch (Figure S8A). Additionally, interassay analysis of six different biosensor batches under identical experimental conditions revealed an RSD of 3.6% in electrochemical signal response (Figure S8B), demonstrating the biosensor's excellent reproducibility. By integrating CRISPR/Cas systems with the electrochemical interface, we have developed a CasPS-based electrochemical biosensor capable of detecting target proteases with femtomolar sensitivity.

Versatility in the Analysis of Different Viral Proteases. A key advantage of the CasPS-powered electrochemical biosensor is its remarkable versatility, stemming from its modular design. By strategically fine-tuning the CasPS module with different proteolysis-responsive capacities, electrochemical biosensors for various viral proteases can be fabricated without modifying the electrochemical interface. In our previous study, we constructed $CasPS_{TEV}$ and $CasPS_{3C}$ to detect TEV protease and HRV type 14 3C protease, respectively, utilizing their corresponding substrate peptides as flexible linkers (Figure 4A).[30] The respective protease

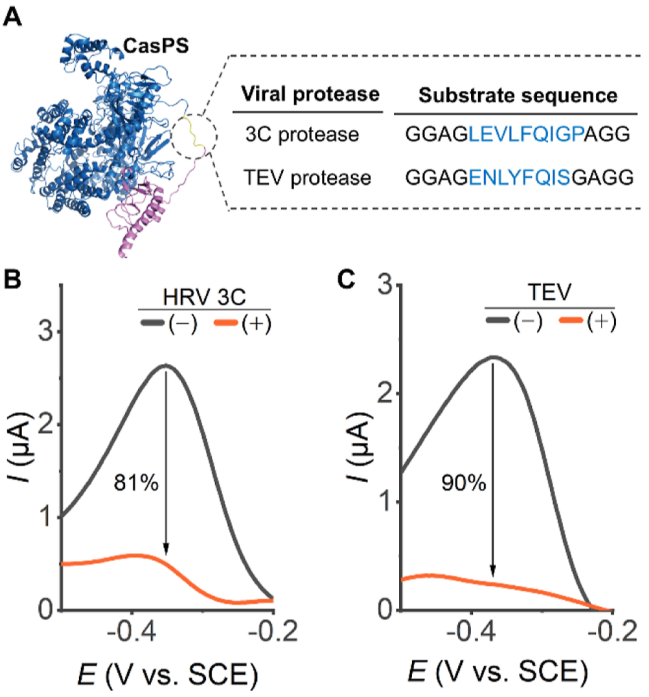


Figure 4. Versatility in the analysis of different viral proteases. (A) Schematic illustration of CasPSs containing various viral protease substrates as linkers. (B) DPV curves of electrochemical biosensors in the absence (gray) and presence (orange) of HRV 3C protease. (C) DPV curves of electrochemical biosensors in the absence (gray) and presence (orange) of TEV protease. Each CasPS, 100 nM; crRNA, 100 nM; dsDNA, 50 nM; HRV 3C protease, 500 nM; and TEV protease, 500 nM.

biosensors were then fabricated by integrating these CasPSs with the electrochemical interface. For $CasPS_{3C}$, the DPV peak current decreased from 2.64 to 0.49 μA upon the treatment with HRV 3C protease, representing an 81% reduction in signal intensity (Figure 4B). Similarly, pretreatment with TEV protease resulted in a 90% signal intensity reduction (Figure 4C). These results demonstrate the good versatility of the CasPS-based electrochemical biosensor for the label-free detection of diverse viral proteases.

Detection of Viral Protease Activity in Virus-Infected Cell Samples. To validate the CasPS-powered electrochemical biosensor's capability for detecting viral protease in complex biological samples with high sensitivity, virus-infected cells were examined (Figure 5A). EV71, a member of the picornaviridae family of small, nonenveloped RNA viruses, is highly contagious in the central nervous system.[43] The virus

https://doi.org/10.1021/acs.analchem.5c00547
Anal. Chem. XXXX, XXX, XXX−XXX

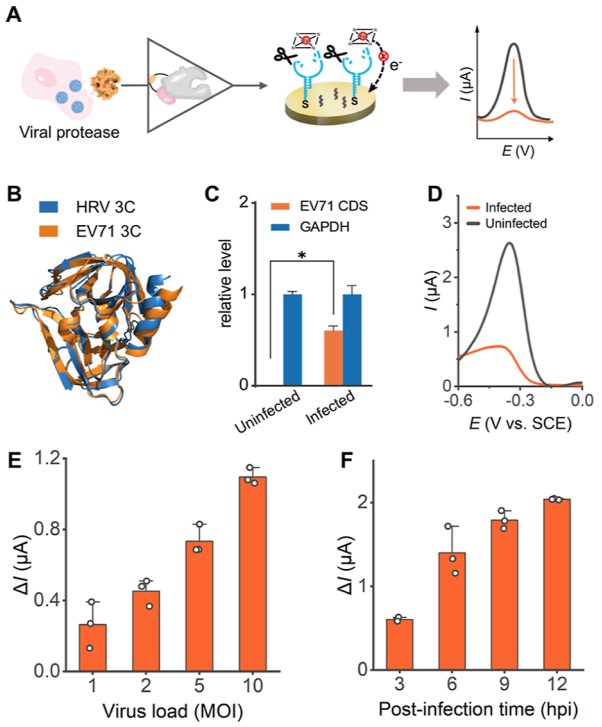


Figure 5. Detection of viral protease activity in virus-infected cell samples. (A) Schematic representation of the detection of 3C protease activity in EV71-infected cells by CasPS-powered electrochemical sensing. (B) Structural analysis of EV71 and HRV 3C protease. (C) Quantification of the relative expression levels of 3C protease mRNA in infected and uninfected HEK293T cells using qPCR. (D) Electrochemical response signals from lysates of infected and uninfected HEK293T cells. (E) Peak DPV signal in HEK293T cells infected by EV71 with varying MOI. (F) Peak DPV signal of HEK293T cells infected by EV71 with different hpi. Data points represent mean ± SD (n = 3).

can cause severe clinical symptoms, including meningitis, encephalitis, poliomyelitis-like paralysis, and potentially fatal complications. The viral 3C protease plays a critical role in multiple pathological processes. Specifically, it has been demonstrated to degrade DNA repair enzymes, thereby activating caspases and inducing host cell apoptosis.[44] Moreover, the protease suppresses innate immunity by inhibiting the type I interferon response.[45] As a key component of EV71 in host cells, the 3C protease is crucial for viral replication and apoptosis, making it a valuable target for viral detection and antiviral drug design.[46,47]

Sequence and structural analyses revealed a high degree of homology between EV71 and HRV 3C proteases (Figures 5B and S9). More importantly, both proteases recognize substrates sharing 83.3% sequence identity, preserving the essential LFQ↓GP core motif required for catalytic activity.[48,49] Therefore, $CasPS_{3C}$ could serve as an effective module for sensing EV71 3C protease activity. Using HEK293T cells as a model, we explored the electrochemical biosensor's effectiveness in assessing EV71 3C protease activity post-infection. The infection efficacy was confirmed through quantitative real-time PCR (Figures 5C and S10). Upon analyzing lysed cells using the CasPS-powered electrochemical biosensor, a significant difference in DPV peak current between infected and uninfected cells was observed (Figure 5D).

In infectious disease clinical practice and research, viral load and exposure time are critical determinants that profoundly influence disease progression and clinical outcomes.[50] Consequently, we investigated the utility of the CasPS-powered electrochemical biosensor for detecting virus-infected cells with varying viral loads and infection dynamics. Using HEK293T cells infected with EV71 at multiplicities of infection (MOI) ranging from 1 to 10, we observed a significant correlation between response signals and viral load in DPV peak current (Figures 5E and S11). To comprehensively assess the assay's feasibility, we monitored dynamic 3C protease changes by examining infected cells at different hours postinfection (hpi). As depicted in Figures 5F and S12, response signals demonstrated a consistent and progressive increase from 3 to 12 hpi. Notably, the expression level of 3C protease in cell lysates escalated proportionally with post-infection time, aligning with established literature. These findings substantiate our biosensor's potential for monitoring viral protease activity in EV71 infection cell models and underscore its promising applications in clinical surveillance of viral infection.

CONCLUSIONS

In conclusion, we have developed a CasPS-powered label-free electrochemical sensor for ultrasensitive viral protease detection. By leveraging the hemin aptamer as an innovative signal reporting probe for CRISPR/Cas12a, we established a label-free electrochemical biosensing interface. Through the strategic integration of the protease-responsive CasPS with the hemin aptamer-based electrochemical interface, we developed a label-free electrochemical biosensor for the analysis of viral proteases. Owing to the efficient coupling of CRISPR/Cas12a-mediated signal amplification and advanced electrochemical detection, this CasPS-powered sensor achieved specific viral protease detection with femtomolar sensitivity. By modularly replacing the CasPS component, we successfully developed electrochemical biosensors targeting diverse viral proteases. Furthermore, the sensor's feasibility was validated by sensitively assessing EV71 3C protease levels in cell lysates across varying viral loads and infection times, underscoring its potential applications in viral infection diagnostics and antiviral drug screening. Ultimately, this work presents a promising strategy for integrating CRISPR biosensing with electrochemical platforms, offering helpful tools for infectious disease research.

ASSOCIATED CONTENT

Supporting Information

The Supporting Information is available free of charge at https://pubs.acs.org/doi/10.1021/acs.analchem.5c00547.

A detailed description of the experimental procedures; nucleic acid sequence and preparation; colorimetric measurements; verification of proteolysis of CasPS; sequence analysis, and more detailed results (PDF)

AUTHOR INFORMATION

Corresponding Authors

Xiaohua Zhu − *State Key Laboratory of Chemo and Biosensing, College of Chemistry and Chemical Engineering, Hunan Provincial Key Laboratory of Biomacromolecular Chemical Biology, Hunan University, Changsha 410082, P. R. China; Key Laboratory of Chemical Biology and*

https://doi.org/10.1021/acs.analchem.5c00547
Anal. Chem. XXXX, XXX, XXX−XXX

Traditional Chinese Medicine Research (Ministry of Education), College of Chemistry and Chemical Engineering, Hunan Normal University, Changsha 410081, P. R. China; Email: zhuxiaohua@hunnu.edu.cn

Chunyang Lei − *State Key Laboratory of Chemo and Biosensing, College of Chemistry and Chemical Engineering, Hunan Provincial Key Laboratory of Biomacromolecular Chemical Biology, Hunan University, Changsha 410082, P. R. China*; orcid.org/0000-0002-3078-5553; Email: cylei@hnu.edu.cn

Authors

Tianyi Zhang − *State Key Laboratory of Chemo and Biosensing, College of Chemistry and Chemical Engineering, Hunan Provincial Key Laboratory of Biomacromolecular Chemical Biology, Hunan University, Changsha 410082, P. R. China*

Yingying Zhao − *Key Laboratory of Chemical Biology and Traditional Chinese Medicine Research (Ministry of Education), College of Chemistry and Chemical Engineering, Hunan Normal University, Changsha 410081, P. R. China*

Cong Zhu − *State Key Laboratory of Chemo and Biosensing, College of Chemistry and Chemical Engineering, Hunan Provincial Key Laboratory of Biomacromolecular Chemical Biology, Hunan University, Changsha 410082, P. R. China*

Xi Zhu − *Hunan Provincial Key Laboratory of Medical Virology, Institute of Pathogen Biology and Immunology, College of Biology, Hunan University, Changsha 410082, P. R. China*

Ye Qiu − *Hunan Provincial Key Laboratory of Medical Virology, Institute of Pathogen Biology and Immunology, College of Biology, Hunan University, Changsha 410082, P. R. China*

Zhou Nie − *State Key Laboratory of Chemo and Biosensing, College of Chemistry and Chemical Engineering, Hunan Provincial Key Laboratory of Biomacromolecular Chemical Biology, Hunan University, Changsha 410082, P. R. China*; orcid.org/0000-0001-9864-2965

Complete contact information is available at: https://pubs.acs.org/10.1021/acs.analchem.5c00547

Author Contributions

[‖]T.Z. and Y.Z. authors contributed equally to this manuscript. The manuscript was written with the contributions of all authors. All authors have given approval to the final version of the manuscript.

Notes

The authors declare no competing financial interest.

■ ACKNOWLEDGMENTS

This work was supported by the National Key R&D Program of China (2024YFA0916700), the National Natural Science Foundation of China (22374036, 22422404, 22034002), and the National Natural Science Foundation of Hunan Province (2023ZJ1120). X.Z. thanked the support from China Postdoctoral Science Foundation (2023M731053).

■ REFERENCES

(1) Lu, L.; Su, S.; Yang, H.; Jiang, S. *Cell* **2021**, *184*, 1604−1620.
(2) Tang, Z.; Kong, N.; Zhang, X.; Liu, Y.; Hu, P.; Mou, S.; Liljeström, P.; Shi, J.; Tan, W.; Kim, J. S.; Cao, Y.; Langer, R.; Leong, K. W.; Farokhzad, O. C.; Tao, W. *Nat. Rev. Mater.* **2020**, *5*, 847−860.
(3) von Delft, A.; Hall, M. D.; Kwong, A. D.; Purcell, L. A.; Saikatendu, K. S.; Schmitz, U.; Tallarico, J. A.; Lee, A. A. *Nat. Rev. Drug Discovery* **2023**, *22*, 585−603.
(4) Nitsche, C.; Holloway, S.; Schirmeister, T.; Klein, C. D. *Chem. Rev.* **2014**, *114*, 11348−11381.
(5) Agol, V. I.; Gmyl, A. P. *Nat. Rev. Microbiol.* **2010**, *8*, 867−878.
(6) Steiner, S.; Kratzel, A.; Barut, G. T.; Lang, R. M.; Aguiar Moreira, E.; Thomann, L.; Kelly, J. N.; Thiel, V. *Nat. Rev. Microbiol.* **2024**, *22*, 206−225.
(7) Tong, L. *Chem. Rev.* **2002**, *102*, 4609−4626.
(8) Tsu, B. V.; Fay, E. J.; Nguyen, K. T.; Corley, M. R.; Hosuru, B.; Dominguez, V. A.; Daugherty, M. D. *Front. Immunol.* **2021**, *12*, 769543.
(9) Yuan, S.; Fan, K.; Chen, Z.; Sun, Y.; Hou, H.; Zhu, L. *Virol. Sin.* **2020**, *35*, 445−454.
(10) Butt, A. A.; Kanwal, F. *Clin. Infect. Dis.* **2012**, *54*, 96−104.
(11) Miura, T.; Malla, T. R.; Owen, C. D.; Tumber, A.; Brewitz, L.; McDonough, M. A.; Salah, E.; Terasaka, N.; Katoh, T.; Lukacik, P.; Strain-Damerell, C.; Mikolajek, H.; Walsh, M. A.; Kawamura, A.; Schofield, C. J.; Suga, H. *Nat. Chem.* **2023**, *15*, 998−1005.
(12) Li, G.; Hilgenfeld, R.; Whitley, R.; De Clercq, E. *Nat. Rev. Drug Discovery* **2023**, *22*, 449−475.
(13) Dutta, R.; Makhaik, S.; Zhao, P.; Cruz, K. G.; Park, K.-W.; Liu, H.; Andrew, T. L.; Hardy, J. A.; Thayumanavan, S. *Anal. Chem.* **2022**, *94*, 12699−12705.
(14) Jin, Z.; Mantri, Y.; Retout, M.; Cheng, Y.; Zhou, J.; Jorns, A.; Fajtova, P.; Yim, W.; Moore, C.; Xu, M.; Creyer, M. N.; Borum, R. M.; Zhou, J.; Wu, Z.; He, T.; Penny, W. F.; O'Donoghue, A. J.; Jokerst, J. V. *Angew. Chem., Int. Ed.* **2022**, *61*, No. e202112995.
(15) Pandit, S.; Duchow, M.; Chao, W.; Capasso, A.; Samanta, D. *Angew. Chem., Int. Ed.* **2024**, *63*, No. e202310964.
(16) Rodriguez-Rios, M.; Megia-Fernandez, A.; Norman, D. J.; Bradley, M. *Chem. Soc. Rev.* **2022**, *51*, 2081−2120.
(17) Ma, T.; Hou, Y.; Zeng, J.; Liu, C.; Zhang, P.; Jing, L.; Shangguan, D.; Gao, M. *J. Am. Chem. Soc.* **2018**, *140*, 211−218.
(18) Zhang, S.; Shi, W.; Li, K. B.; Han, D. M.; Xu, J. J. *Anal. Chem.* **2022**, *94*, 4407−4416.
(19) Capelli, L.; Pedrini, F.; Di Pede, A. C.; Chamorro-Garcia, A.; Bagheri, N.; Fortunati, S.; Giannetto, M.; Mattarozzi, M.; Corradini, R.; Porchetta, A.; Bertucci, A. *Anal. Chem.* **2024**, *96*, 18645−18654.
(20) Tian, T.; Zhou, X. *Annu. Rev. Anal. Chem.* **2023**, *16*, 311−332.
(21) Tang, Y.; Gao, L.; Feng, W.; Guo, C.; Yang, Q.; Li, F.; Le, X. C. *Chem. Soc. Rev.* **2021**, *50*, 11844−11869.
(22) Wan, Y.; Zong, C.; Li, X.; Wang, A.; Li, Y.; Yang, T.; Bao, Q.; Dubow, M.; Yang, M.; Rodrigo, L.-A.; Mao, C. *Chem. Rev.* **2022**, *122*, 8126−8180.
(23) Chen, J. S.; Ma, E.; Harrington, L. B.; Da Costa, M.; Tian, X.; Palefsky, J. M.; Doudna, J. A. *Science* **2018**, *360*, 436−439.
(24) Liu, X.; Yang, H.; Liu, J.; Liu, K.; Jin, L.; Zhang, Y.; Khan, M. R.; Zhong, K.; Cao, J.; He, Q.; Xia, X.; et al. *Anal. Chem.* **2024**, *96*, 2032−2040.
(25) Feng, W.; Zhang, H.; Le, X. C. *Anal. Chem.* **2023**, *95*, 206−217.
(26) Chen, S.; Gong, B.; Zhu, C.; Lei, C.; Nie, Z. *TrAC, Trends Anal. Chem.* **2023**, *159*, 116931.
(27) Wang, K.; Liu, S.; Zhou, S.; Qileng, A.; Wang, D.; Liu, Y.; Chen, C.; Lei, C.; Nie, Z. *Angew. Chem., Int. Ed.* **2025**, *64*, No. e202416671.
(28) Chen, S.; Wang, R.; Peng, S.; Xie, S.; Lei, C.; Huang, Y.; Nie, Z. *Chem. Sci.* **2022**, *13*, 2011−2020.
(29) Xiong, Y.; Zhang, J.; Yang, Z.; Mou, Q.; Ma, Y.; Xiong, Y.; Lu, Y. *J. Am. Chem. Soc.* **2020**, *142*, 207−213.
(30) Kang, W.; Xiao, F.; Zhu, X.; Ling, X.; Xie, S.; Li, R.; Yu, P.; Cao, L.; Lei, C.; Qiu, Y.; Liu, T.; Nie, Z. *Angew. Chem., Int. Ed.* **2024**, *63*, No. e202400599.
(31) Yu, P.; Lei, C.; Nie, Z. *J. Electroanal. Chem.* **2022**, *911*, 116209.
(32) Dai, Y.; Somoza, R. A.; Wang, L.; Welter, J. F.; Li, Y.; Caplan, A. I.; Liu, C. C. *Angew. Chem., Int. Ed.* **2019**, *58*, 17399−17405.
(33) Qing, M.; Chen, S. L.; Sun, Z.; Fan, Y.; Luo, H. Q.; Li, N. B. *Anal. Chem.* **2021**, *93*, 7499−7507.

(34) Castro, A. C. H.; Bezerra, I. R. S.; Pascon, A. M.; Da Silva, G. H.; Philot, E. A.; De Oliveira, V. L.; Mancini, R. S. N.; Schleder, G. R.; Castro, C. E.; De Carvalho, L. R. S.; Fernandes, B. H. V.; Cilli, E. M.; Sanches, P. R. S.; Santhiago, M.; Charlie-Silva, I.; Martinez, D. S. T.; Scott, A. L.; Alves, W. A.; Lima, R. S. *ACS Nano* **2022**, *16*, 14239−14253.
(35) Liu, F.; Yang, M.; Song, W.; Luo, X.; Tang, R.; Duan, Z.; Kang, W.; Xie, S.; Liu, Q.; Lei, C.; Huang, Y.; Nie, Z.; Yao, S. *Chem. Sci.* **2020**, *11*, 2993−2998.
(36) Zhang, C.; Ku, Z.; Liu, Q.; Wang, X.; Chen, T.; Ye, X.; Li, D.; Jin, X.; Huang, Z. *Vaccine* **2015**, *33*, 2335−2341.
(37) Huang, S.; Lou, Y.; Zheng, L. *Nucleic Acids Res.* **2024**, *52*, 11148−11157.
(38) Gu, L.; Ding, Y.; Zhou, Y.; Zhang, Y.; Wang, D.; Liu, J. *Angew. Chem., Int. Ed.* **2024**, *63*, No. e202314450.
(39) Rossetti, M.; Merlo, R.; Bagheri, N.; Moscone, D.; Valenti, A.; Saha, A.; Arantes, P. R.; Ippodrino, R.; Ricci, F.; Treglia, I.; Delibato, E.; van der Oost, J.; Palermo, G.; Perugino, G.; Porchetta, A. *Nucleic Acids Res.* **2022**, *50*, 8377−8391.
(40) Zhu, X.; Fan, L.; Wang, S.; Lei, C.; Huang, Y.; Nie, Z.; Yao, S. *Anal. Chem.* **2018**, *90*, 6742−6748.
(41) Yu, Y.; Guo, Q.; Jiang, W.; Zhang, H.; Cai, C. *Anal. Chem.* **2021**, *93*, 11298−11304.
(42) Shi, K.; Cao, L.; Liu, F.; Xie, S.; Wang, S.; Huang, Y.; Lei, C.; Nie, Z. *Biosens. Bioelectron.* **2021**, *190*, 113372.
(43) Yamayoshi, S.; Yamashita, Y.; Li, J.; Hanagata, N.; Minowa, T.; Takemura, T.; Koike, S. *Nat. Med.* **2009**, *15*, 798−801.
(44) Li, M.-L.; Hsu, T.-A.; Chen, T.-C.; Chang, S.-C.; Lee, J.-C.; Chen, C.-C.; Stollar, V.; Shih, S.-R. *Virology* **2002**, *293*, 386−395.
(45) Mukherjee, A.; Morosky, S. A.; Delorme-Axford, E.; Dybdahl-Sissoko, N.; Oberste, M. S.; Wang, T.; Coyne, C. B. *PLoS Pathog.* **2011**, *7*, No. e1001311.
(46) Liu, M.; Xu, B.; Ma, Y.; Shang, L.; Ye, S.; Wang, Y. *Antiviral Res.* **2021**, *192*, 105102.
(47) Lu, G.; Qi, J.; Chen, Z.; Xu, X.; Gao, F.; Lin, D.; Qian, W.; Liu, H.; Jiang, H.; Yan, J.; Gao, G. F. *J. Virol.* **2011**, *85*, 10319−10331.
(48) Kuo, C.-J.; Shie, J.-J.; Fang, J.-M.; Yen, G.-R.; Hsu, J. T.-A.; Liu, H.-G.; Tseng, S.-N.; Chang, S.-C.; Lee, C.-Y.; Shih, S.-R.; Liang, P.-H. *Bioorg. Med. Chem.* **2008**, *16*, 7388−7398.
(49) Fan, X.; Li, X.; Zhou, Y.; Mei, M.; Liu, P.; Zhao, J.; Peng, W.; Jiang, Z.-B.; Yang, S.; Iverson, B. L.; Zhang, G.; Yi, L. *ACS Chem. Biol.* **2020**, *15*, 63−73.
(50) Puhach, O.; Meyer, B.; Eckerle, I. *Nat. Rev. Microbiol.* **2023**, *21*, 147−161.

https://doi.org/10.1021/acs.analchem.5c00547
Anal. Chem. XXXX, XXX, XXX−XXX